SUPPORTING INFORMATION

Interplay between charge carrier mobility, exciton diffusion, crystal packing and charge separation in perylene diimide-based heterojunctions

*Kevin M. Felter[1], Valentina M. Caselli[1], D. Deniz Günbaş[1,2], Tom J. Savenije[1] and Ferdinand C. Grozema[1]**

1 Opto-electronic Materials Section, Department of Chemical Engineering, Faculty of Applied Sciences, Delft University of Technology, Van der Maasweg 9, 2629 HS Delft, the Netherlands

2 Present address: SABIC Netherlands, Bergen op Zoom, The Netherlands

Email: F.C.Grozema@tudelft.nl

1. Dektak – Target and measured PDI film thicknesses

The thickness of the evaporated PDI thin films were measured with a *Dektak* profilometer. Ten scans were made and averaged for every sample and consisted of measuring over the step from clean silica to the PDI layer. The height offset indicates the film thickness. We call the thickness set in the evaporator the nominal thickness and the measured film thickness the real film thickness.

Table S1 Overview of the target (nominal) thin film thicknesses as set in the evaporator and the measured (real) thicknesses of the PDI-octyl and PDI-hexhep thin films.

PDI-octyl thickness		PDI-hexhep thickness	
Nominal (nm)	Real (nm)	Nominal (nm)	Real (nm)
15	17.5	30	49.2
30	26.5	50	49.9
50	41.9	100	82.8
100	67.6	150	166.8
150	112.8	250	232.9
250	167.9		
500	326.7		

2. Thin film crystallite domain size estimation using the Scherrer equation

We estimated the domain size of crystallites τ from our XRD measurements using the Scherrer equation:

$$\tau = \frac{K\lambda}{\beta \cos\theta} \qquad \text{(S1)}$$

Where K is the shape factor which is a function of crystallite shape and assumed to be 0.94, λ is the wavelength of the X-ray radiation (0.179 nm), β (in radians) is the Full Width Half Maximum (FWHM) location of the analysed reflection minus broadening caused by the instrument and θ (in radians) is the angle of reflection. Using this equation on the reflection observed in the XRD spectra of the thin films shown in Figure 3 we can calculate the crystallite domain size values shown in Table S2. The crystallite packing of PDI-octyl is shown in Figure S1 and is the molecular cell containing the intact contents of one unit cell. For PDI-hexhep this image cannot be shown as its crystalline structure is not available.

Table S2 Crystallite grain sizes for the thin films of various thickness of PDI-octyl and PDI-hexhep as determined using the Scherrer equation.

Film thickness (nm)	PDI-octyl			PDI-hexhep		
	β (°)	θ (°)	τ (nm)	β (°)	θ (°)	τ (nm)
30	0.370	4.971	27.7	0.358	5.829	28.6
50	0.316	5.063	32.5	0.238	5.845	43.2
100	0.169	5.091	60.9	0.128	5.846	80.2
150	0.127	5.096	80.8	0.091	5.846	113.0
250	0.106	5.112	97.0	0.078	5.862	131.3

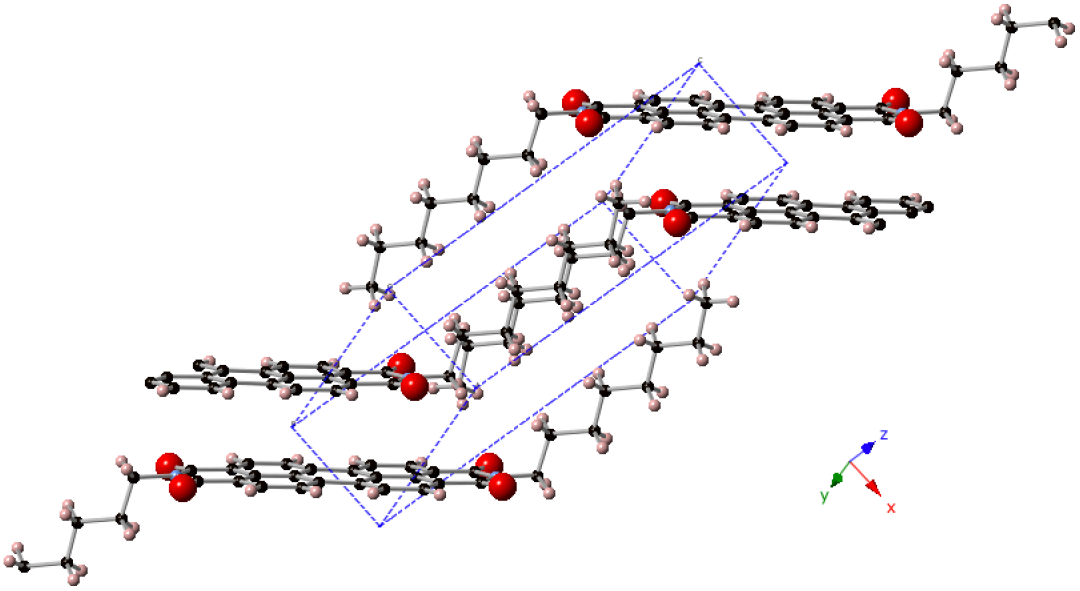

Figure S1 Image of the molecular cell of PDI-octyl showing the unit cell (blue dash) and the molecule unit it contains in an intact shape. This image shows the molecular packing of PDI-octyl.

3. SEM images of 30 nm and 100 nm thick annealed PDI layers on fused silica

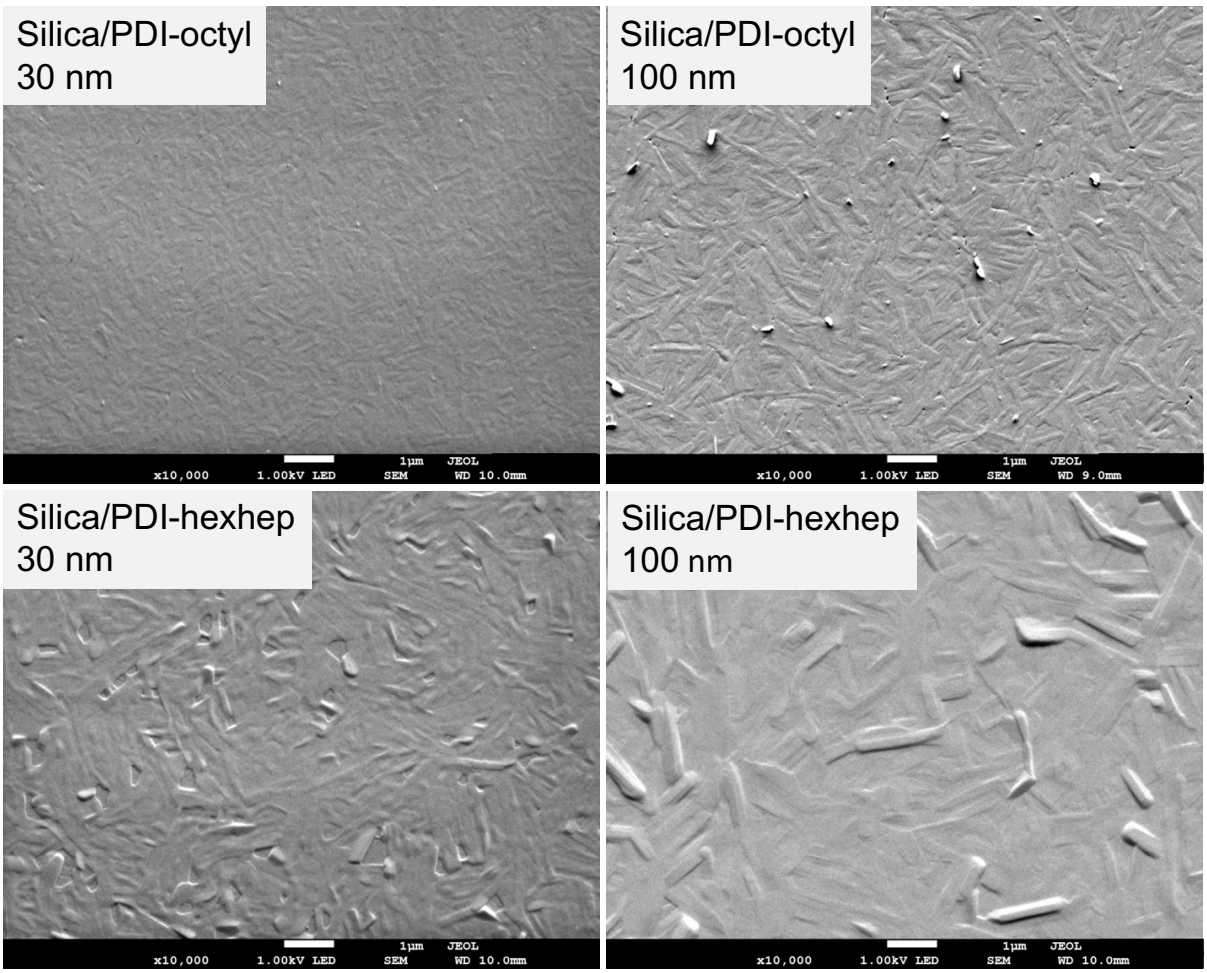

Figure S2 SEM images of a 30 and 100 nm annealed thin film of PDI-octyl (left panel) and PDI-hexhep (right panel). Scale bars indicate the size of the features at 10.000X magnification. The samples are coated with a 3 nm Pt layer.

4. SEM images of uncoated fused silica and TiO_2 layers on fused silica

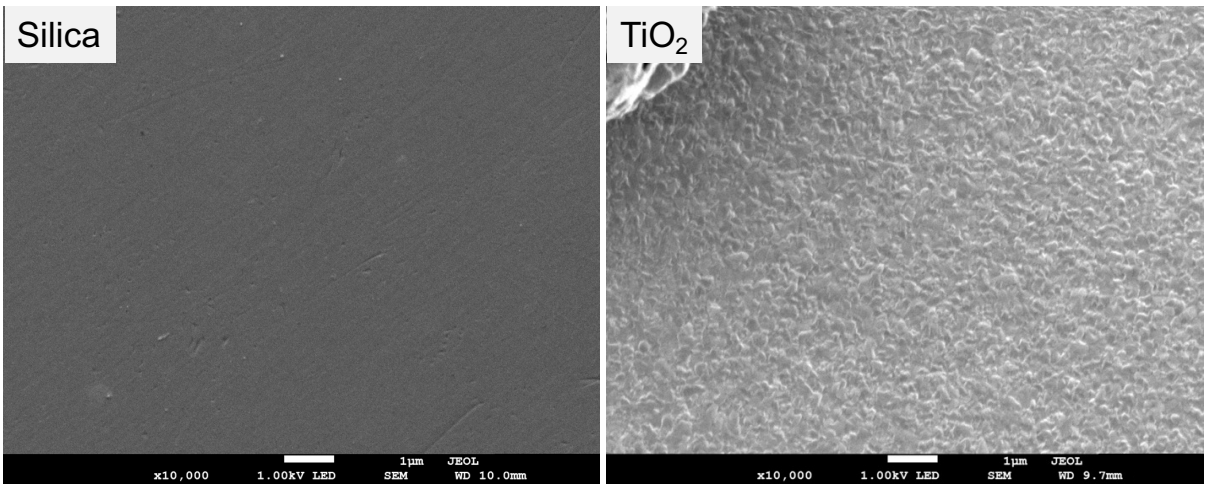

Figure S3 SEM images of an uncoated fused silica substrate and a TiO_2 coated fused silica substrate as used in this study at 10.000X magnification. The samples are coated with a 3 nm Pt layer.

5. Optical properties of PDI-octyl, PDI-hexhep and ZnPc

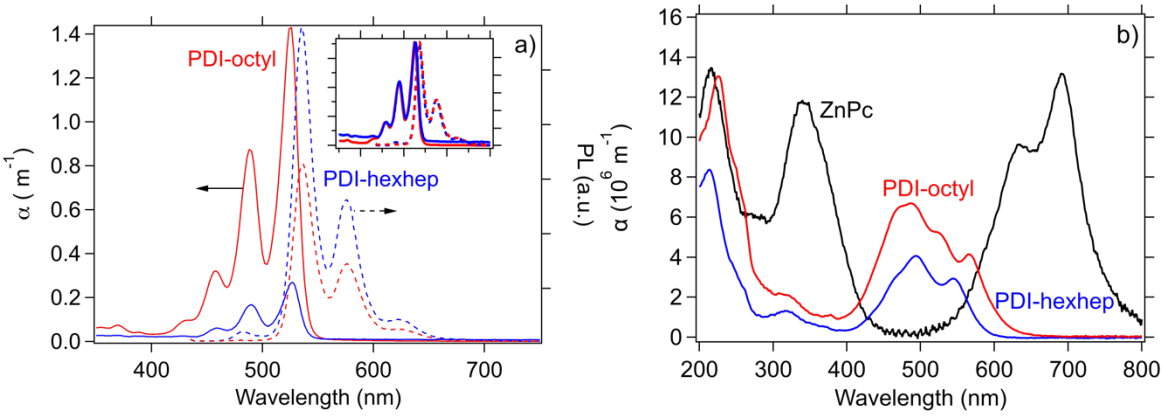

Figure S4 a) Absorption spectra of PDI-octyl and PDI-hexhep in a $1 \cdot 10^{-5}$ M $CHCl_3$ solution and b) solid-state absorption spectra of a PDI-octyl (50 nm), PDI-hexhep (50 nm) and ZnPc (30 nm) individual layers.

6. XRD of TiO_2/PDI heterojunctions

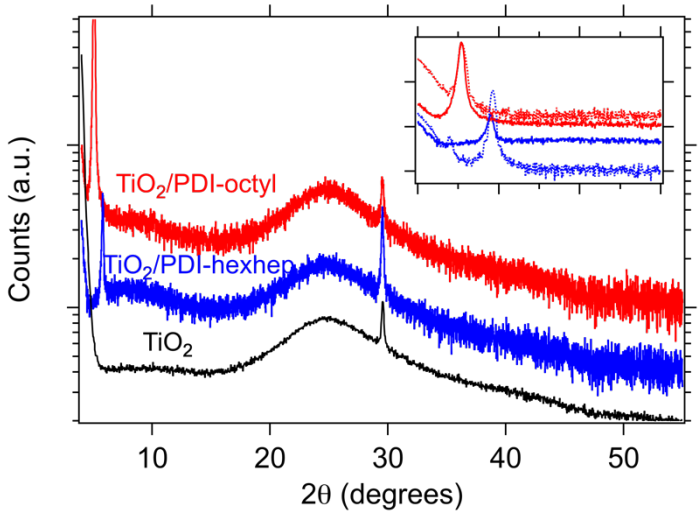

Figure S5 XRD diffractograms of a TiO_2/PDI-octyl (red) and TiO_2/PDI-hexhep (blue) heterojunction and a TiO_2 sample. The reflection at 29 2θ originates from the TiO_2. The inset shows that the PDI reflection on TiO_2 (solid line) has an identical width and position as on fused silica (dotted line).

7. TRMC photon fluence dependence charge carrier kinetics for PDI-octyl

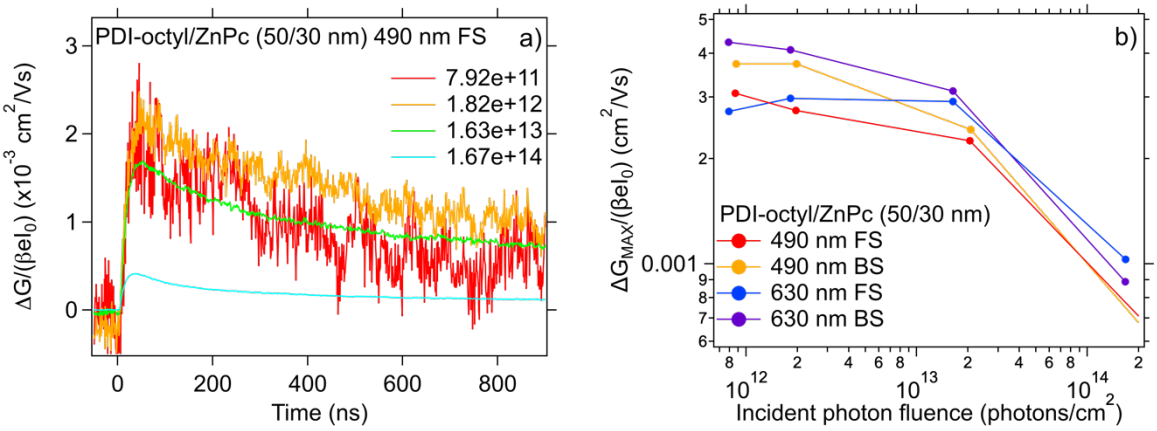

Figure S6 a) Photoconductivity transients for a 50/30 nm PDI-octyl/ZnPc bilayer at various photon fluences upon 490 nm FS excitation. b) The photon fluence dependence of $\eta_0\Sigma\mu$ for the same bilayer upon PDI (490 nm) and ZnPc (630 nm) at FS and BS.

8. Table with kinetic parameters obtained from fitting of PDI-octyl TRMC transients

The estimation of the exciton diffusion length requires a correction for possible electron-hole recombination that occurs within the instrumental response time. This correction is carried out by fitting the transients with a tri-exponential function as described by equation 9. Some of the fitting parameters are time constants that describe charge carrier decay processes and are obtained with their respective weight. In addition, we obtain an estimate for the intrinsic change in photoconductance ΔG_0. We provide these fitting parameters in Table S3 as function of film thickness, excitation side (front side FS, backside BS) and excitation wavelength (490 nm PDI excitation and 630 nm ZnPc excitation) for PDI-octyl. We use the ΔG_0 values to determine the exciton diffusion length.

Table S3 Fitting parameters obtained from a tri-exponential it on the photoconductivity transients of PDI-octyl/ZnPc as function of different PDI-octyl thicknesses and illumination side (FS = front side and BS = back side) dependence at 490 and 630 nm excitation.

PDI-octyl/ZnPc

490 nm

	Side	PF	τ_1	τ_2	τ_3	W_1	W_2	W_3	G_0
15/30	FS	1.94E+12	6.0E-07	8.0E-05	5.0E-04	5.0E-01	3.0E-01	2.0E-01	5.1E-03
	BS	8.05E+11	6.0E-07	8.0E-05	5.0E-04	5.0E-01	3.0E-01	2.0E-01	6.4E-03
30/30	FS	8.77E+11	6.0E-08	9.0E-07	1.0E-06	5.0E-01	4.0E-01	1.0E-01	2.6E-03
	BS	8.67E+11	1.0E-07	8.0E-07	1.0E-05	5.0E-01	4.0E-01	1.0E-01	3.0E-03
50/30	FS	8.65E+11	6.0E-08	7.0E-07	1.0E-06	5.0E-01	4.0E-01	1.0E-01	2.8E-03
	BS	8.74E+11	1.5E-07	1.0E-06	1.0E-04	5.0E-01	4.0E-01	1.0E-01	3.7E-03
100/30	FS	8.59E+11	2.0E-07	1.0E-05	1.0E-04	5.0E-01	4.0E-01	1.0E-01	3.8E-03
	BS	8.36E+11	2.0E-07	5.0E-06	1.0E-05	5.0E-01	4.0E-01	1.0E-01	3.4E-03
150/30	FS	8.83E+11	2.0E-07	2.0E-05	1.0E-04	5.0E-01	4.0E-01	1.0E-01	4.7E-03

	BS	8.29E+11	2.0E-07	6.0E-05	1.0E-04	5.0E-01	4.0E-01	1.0E-01	2.6E-03
250/30	FS	8.35E+11	1.5E-07	1.5E-06	1.0E-04	5.0E-01	4.0E-01	1.0E-01	4.0E-03
	BS	8.26E+11	1.0E-07	6.0E-07	1.0E-05	5.0E-01	4.0E-01	1.0E-01	2.1E-03
500/30	FS	8.87E+11	2.0E-07	5.0E-06	1.0E-04	5.0E-01	4.0E-01	1.0E-01	4.0E-03
	BS	8.25E+11	2.0E-07	3.0E-07	1.0E-06	5.0E-01	4.0E-01	1.0E-01	1.2E-03

630 nm

	Side	**PF**	τ_1	τ_2	τ_3	W_1	W_2	W_3	G_0
15/30	FS								
	BS	6.48E+11	3.5E-07	8.0E-05	5.0E-04	5.0E-01	3.0E-01	2.0E-01	5.7E-03
30/30	FS	7.93E+11	7.0E-08	3.0E-07	1.0E-06	5.0E-01	4.0E-01	1.0E-01	2.5E-03
	BS	7.81E+11	2.0E-07	1.0E-06	1.0E-05	5.0E-01	4.0E-01	1.0E-01	2.2E-03
50/30	FS	7.92E+11	1.5E-07	2.0E-06	1.0E-05	5.0E-01	4.0E-01	1.0E-01	2.2E-03
	BS	7.90E+11	1.0E-07	1.0E-06	5.0E-06	5.0E-01	4.0E-01	1.0E-01	4.0E-03
100/30	FS	7.99E+11	1.5E-07	8.0E-06	1.0E-05	5.0E-01	4.0E-01	1.0E-01	2.8E-03
	BS	7.84E+11	2.0E-07	7.0E-06	1.0E-05	5.0E-01	4.0E-01	1.0E-01	4.6E-03
150/30	FS	7.99E+11	1.0E-07	2.0E-06	1.0E-05	5.0E-01	4.0E-01	1.0E-01	3.8E-03
	BS	8.16E+11	1.5E-07	7.0E-05	1.0E-04	4.0E-01	5.0E-01	1.0E-01	4.3E-03
250/30	FS	7.70E+11	1.0E-07	2.0E-06	1.0E-05	5.0E-01	4.0E-01	1.0E-01	3.8E-03
	BS	7.24E+11	1.0E-07	2.0E-06	1.0E-05	5.0E-01	4.0E-01	1.0E-01	5.5E-03
500/30	FS	7.91E+11	1.0E-07	3.0E-06	1.0E-04	5.0E-01	4.0E-01	1.0E-01	4.2E-03
	BS	7.74E+11	3.0E-07	3.0E-06	1.0E-04	5.0E-01	4.0E-01	1.0E-01	5.2E-03

9. TRMC charge carrier kinetics for PDI-hexhep thin films of variable thickness

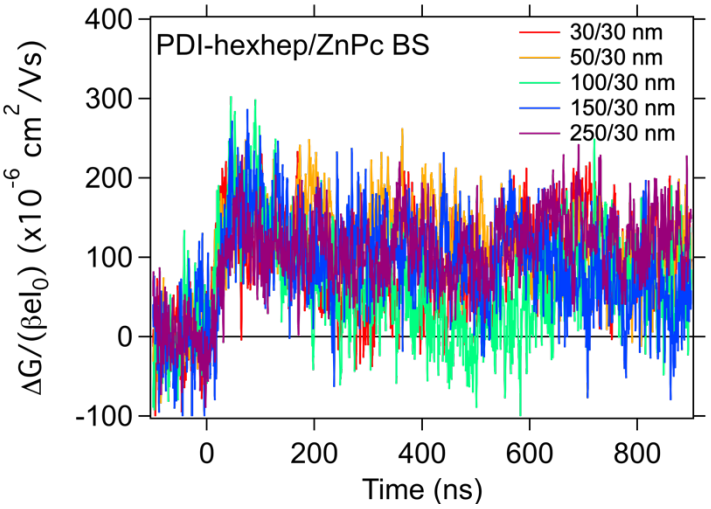

Figure S7 Photoconductivity transients for PDI-hexhep/ZnPc heterojunctions of varying PDI thicknesses. The transients were obtained upon 495 backside excitation (BS) at a photon fluence I_0 of $9.2 \cdot 10^{12}$ photons/cm^2.

10. Methodology for exciton diffusion length determination

The fraction of charges that arrive at the interface *S* for the PDI/ZnPc heterojunction is described by the following two expressions assuming quenching of excitons at the PDI-fused silica interface:

$$S_{FS} = \left(\frac{\alpha^2 \Lambda_{exc}^2}{\alpha^2 \Lambda_{exc}^2 - 1} \right) \left(1 - e^{\alpha L} \operatorname{sech}\left(\frac{L}{\Lambda_{exc}} \right) - \frac{tanh\left(\frac{L}{\Lambda_{exc}} \right)}{\alpha \Lambda_{exc}} \right) \quad \text{(S2a)}$$

$$S_{BS} = \left(\frac{\alpha^2 \Lambda_{exc}^2}{\alpha^2 \Lambda_{exc}^2 - 1} \right) \left(\operatorname{sech}\left(\frac{L}{\Lambda_{exc}} \right) - e^{\alpha L} \left(1 + \frac{tanh\left(\frac{L}{\Lambda_{exc}} \right)}{\alpha \Lambda_{exc}} \right) \right) \quad \text{(S2b)}$$

For the TiO_2/PDI heterojunction we use the following two expressions for S and assume exciton quenching occurs at the PDI-air interface.

$$S_{Q,FS} = \left(\frac{\alpha^2 \Lambda_{exc}^2}{\alpha^2 \Lambda_{exc}^2 - 1} \right) \left(\frac{\operatorname{csch}\left(\frac{L}{\Lambda_{exc}} \right) - e^{\alpha L} \coth\left(\frac{L}{\Lambda_{exc}} \right)}{\alpha \Lambda_{exc}} - e^{\alpha L} \right) \tag{S3a}$$

$$S_{Q,BS} = \left(\frac{\alpha^2 \Lambda_{exc}^2}{\alpha^2 \Lambda_{exc}^2 - 1} \right) \left(1 + \frac{e^{\alpha L} \operatorname{csch}\left(\frac{L}{\Lambda_{exc}} \right) - \coth\left(\frac{L}{\Lambda_{exc}} \right)}{\alpha \Lambda_{exc}} \right) \tag{S3b}$$

The reflection corrected $\eta_0 \Sigma \mu$ values obtained at different excitation wavelengths are plotted in Figure S8a and c as function of the corresponding absorption coefficient α) for PDI-octyl and PDI-hexhep, respectively. Different datasets for front side and back side illumination are fitted individually using Equations 11 and S3 and are shown in the same figure. The fitting results are provided in Table 1. Figure S8b and d contain the fit trajectory at larger α values that serve to check whether the fitting function displays the expected $\eta_0 \Sigma \mu(\alpha)$ trend as function of illumination side.

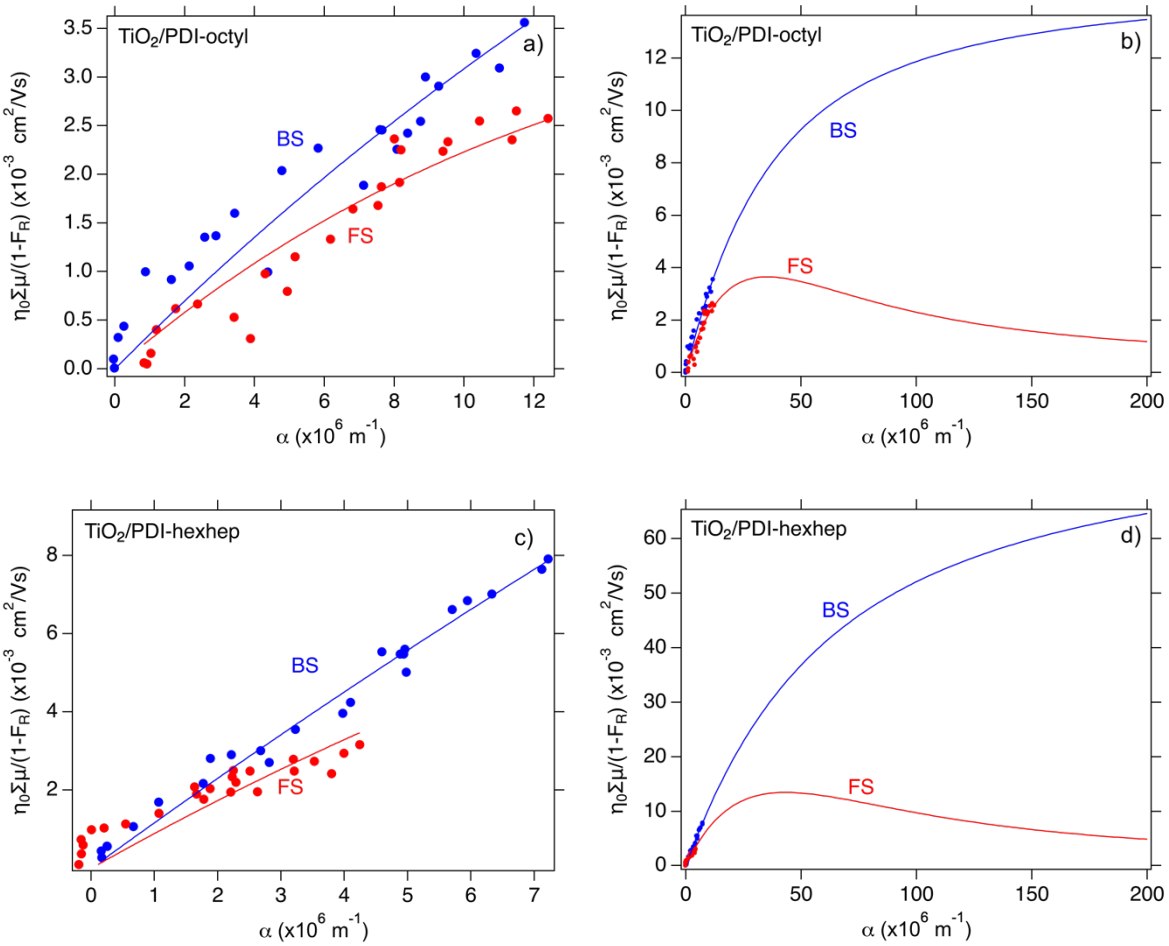

Figure S8 a) A plot of $\eta_0\Sigma\mu$ vs. the absorption coefficient α for a TiO_2/PDI-octyl (100 nm) bilayer upon FS and BS excitation with a fit obtained from applying the exciton diffusion model. c) A plot of $\eta_0\Sigma\mu$ vs. α for a TiO_2/PDI-hexhep (30 nm) bilayer with a fit obtained from applying the exciton diffusion model. b) and d) A plot of the fits at extended values of α to prove a viable exciton diffusion profile, similar to that of the organic bilayer for TiO_2/PDI-octyl and TiO_2/PDI-hexhep, respectively.

11. Determination of the TiO_2 electron mobility

Figure S9a gives a demonstration how the TiO_2 electron mobility was determined. TRMC conductivity fluences were measured at 300 nm backside (BS) TiO_2 excitation. The maximum photoconductance signals at $t = 0$ were plotted as function of fluence and corrected for the fraction of absorbed photons ($F_{A,300nm}$ = 0. 58). The plateau region $\varphi\Sigma\mu$ value was then taken as indicated by the red dashed line in figure S9b. By assuming full exciton charge separation efficiency (φ = 100%) and neglecting any conductivity and thus mobility due to holes, the μ_{e^-} in TiO_2 upon backside excitation was determined as 2.09 cm^2/Vs. In the study we used the average mobility determined upon FS and BS excitation.

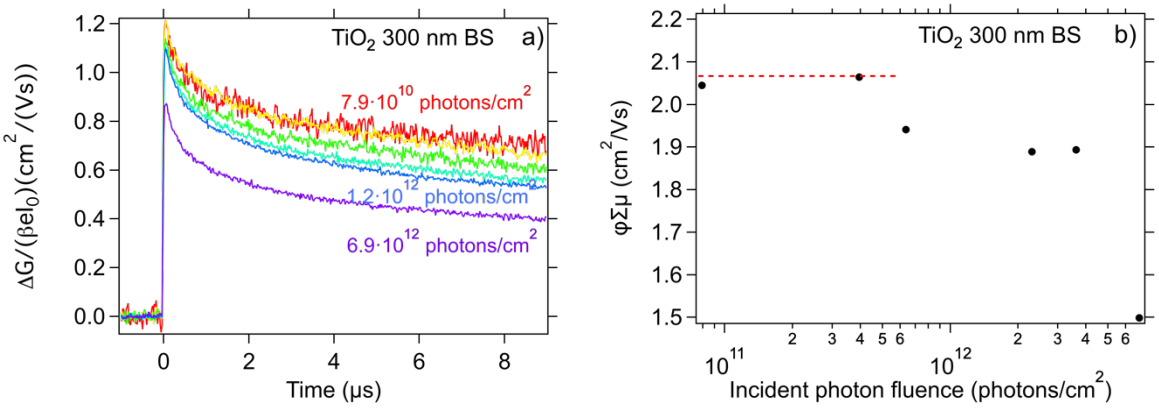

Figure S9 a) TRMC transients of a TiO_2 film upon direct bandgap (300 nm) back side (BS) excitation for the fluence range $1{\cdot}10^9$-$1{\cdot}10^{12}$ photons/cm^2. b) A plot of $\eta\Sigma\mu$ vs. I_0 for the TiO_2 single layer film. The dashed line shows the readout value for the electron mobility in the TiO_2 film.